Astrophysical light scattering problems (PAP316)

Lecture 12a

Karri Muinonen
Academy Professor
Department of Physics, University of Helsinki, Finland

Exoplanets, Contents

Introduction

- Physical characterization of astronomical objects (e.g., surfaces of airless planetary objects)
- Direct problem of light scattering by particles with varying particle size, shape, refractive index, and spatial distribution
- Inverse problem based on astronomical observations and/or experimental measurements
- Plane of scattering, scattering angle, solar phase angle, degree of linear polarization

Searching for exoplanets

- Leading discovery methods indirect:
  - Radial velocity or Doppler method
  - Transit method
- Most sensitive to large exoplanets close to the parent star
  - Large size and short orbital timescales favor detection

Polarimetry for exoplanet detection

- Stokes vector of scattered light:

$$F_s(\lambda,\alpha) = \frac{R_p^{\,2}}{d^2}\frac{1}{4}\boldsymbol{S}(\lambda,\alpha)\pi\boldsymbol{F}_0(\lambda),$$

$$S(\lambda,\alpha) = \begin{bmatrix} a_1(\lambda,\alpha) & b_1(\lambda,\alpha) & 0 & 0 \\ b_1(\lambda,\alpha) & a_2(\lambda,\alpha) & 0 & 0 \\ 0 & 0 & a_3(\lambda,\alpha) & b_2(\lambda,\alpha) \\ 0 & 0 & -b_2(\lambda,\alpha) & a_4(\lambda,\alpha) \end{bmatrix}.$$

- Contrast between exoplanet and parent star reveals challenges in detection

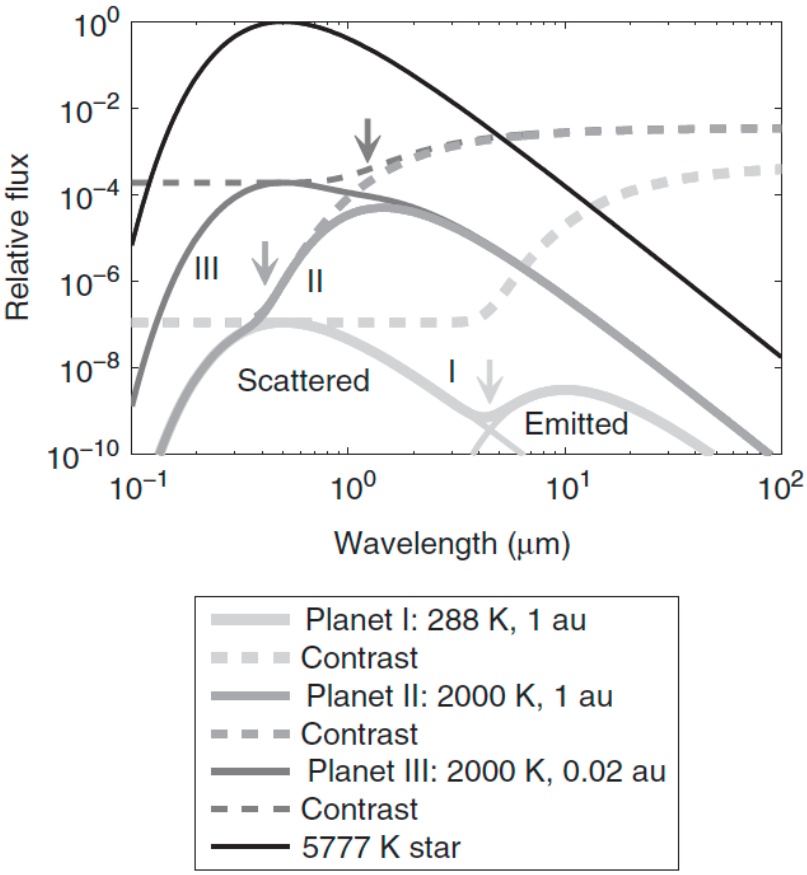

FIGURE 25.1 Black-body spectra of three Jupiter-sized exoplanets in scattered light and in thermal emission. The maximum contrast ratio is of the order of 10^{-4} in scattered light for close-in planets. The maximum contrast ratio in thermal emission is of the order of 10^{-3} for hot planets, which may be hot due to close-in orbits (and therefore buffered by stellar forcing), young ages (hot from recent, rapid formation), or both. The arrows indicate the wavelengths where scattered and thermal fluxes are equal: 4.5 μm (planet I), ~400 nm (planet II), and ~1.2 μm (planet III).

- Full geometry of the exoplanet problem, difficult to illustrate!
- Depending on the geometry, a multitude of polarimetric dependences emerge
- Polarimetry helps tackle the geometry that is likely to be unknown in most cases

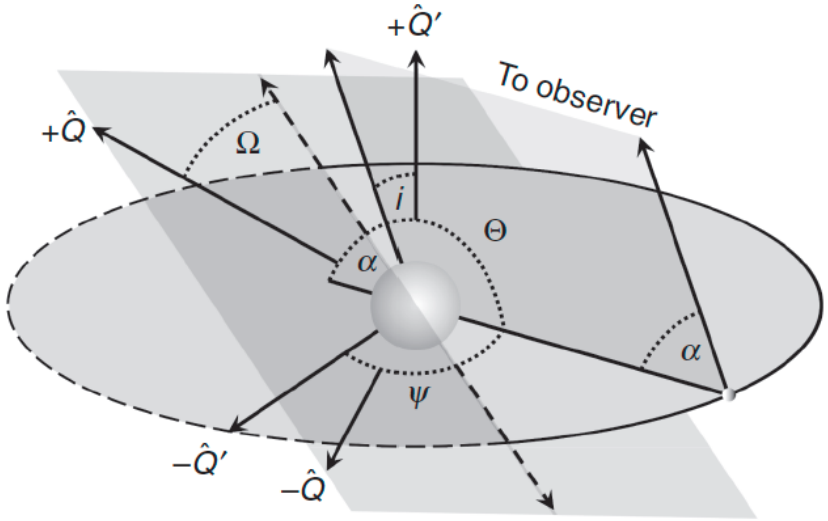

FIGURE 25.2 Geometry of the problem, where phase angle, α, scattering angle, Θ, orbital inclination, i, orbital phase, Ψ, and longitude of the ascending node, Ω, are shown. The orbital plane is given as the ellipse; the scattering plane includes the star, planet, and observer; and the plane of the sky as seen by the observer is the parallelogram centered on the star. The dashed line through the star indicates the line of nodes, which is where the orbital plane intersects the plane of the sky as seen by the observer. The orbital plane pierces the plane of the sky along the line of nodes, where the dashed outline of the orbital plane lies behind the plane of the sky and the solid outline of the orbital plane protrudes from the plane of the sky. The direction $+\hat{Q}'$ is perpendicular to the orbital plane but points toward the observer only in the case of zero inclination, i, where the orbit is seen face-on. For inclinations $i = 90° \pm \arctan(R_*/D)$, the planet will transit its host star at orbital phase $\Psi = 0$ as seen by the observer. The $-\hat{Q}'$ direction lies in the orbital plane. The unprimed directions $+\hat{Q}$ and $-\hat{Q}$ lie in the plane of the sky and indicate celestial north and east, respectively.

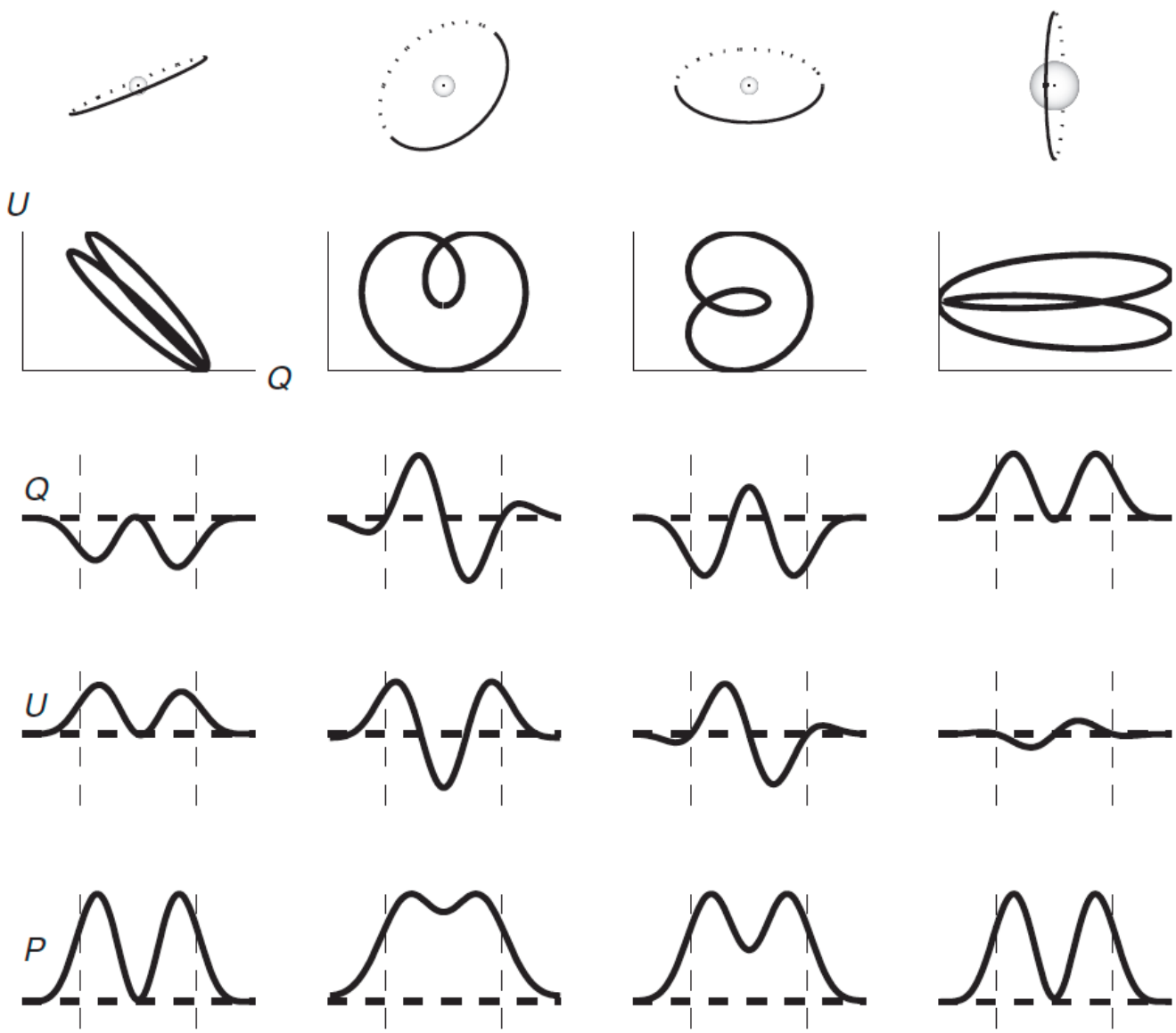

FIGURE 25.3 Orbital modulation of linear Stokes parameters $Q(\Psi)$, $U(\Psi)$, and $P(\psi)=\sqrt{Q(\psi)^2+U(\psi)^2}$ for four hypothetical combinations of orbital inclination i and longitude of the ascending node Ω. Relative sizes between stars and exoplanet orbits are shown to scale for four cases of close-in exoplanets. Solid and dashed curves indicate the orbit of each exoplanet, where solid lines show the orbit protruding toward the observer with respect to the plane of the sky (planet forwardscatters starlight) and dashed lines show the opposite (planet backscatters starlight). The position angle of the line of nodes (the pair of junctions between solid and dashed lines) illustrates Ω.

Polarimetry for exoplanet characterization

- Compare exoplanet characterization to the success with Venus
- Hansen and Hovenier (1974) retrieved Venus atmospheric composition from polarimetric observations by Lyot (1929) and Coffeen and Gehrels (1969)
- Polarimetry will primarily be a characterization tool in exoplanet research

Flux and polarization signals from exoplanets
Signals from gaseous exoplanets

- Lambertian vs. Hilton phase functions
- Rayleigh vs. more complicated linear polarization

$$P(\lambda,\Theta) \propto \sin^2\Theta / \left(1+\cos^2\Theta\right)$$

- Spherical vs. geometric albedo vs. phase integral

$$A_B = A_g \Phi \qquad \Phi = \int_0^{\pi} a_1(\lambda,\alpha)\sin\alpha d\alpha,$$

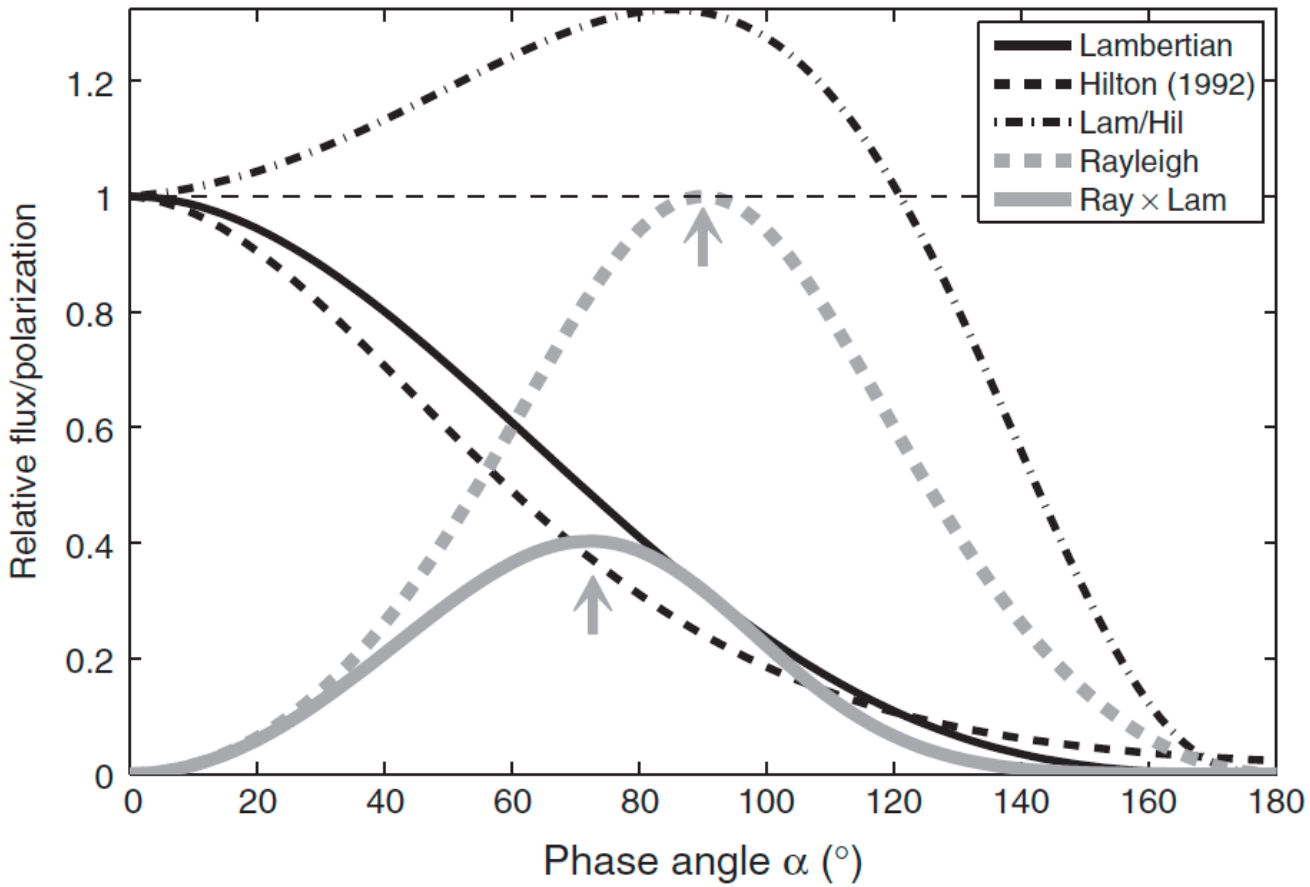

FIGURE 25.4 Expected phase functions (total scattered light flux) for the Lambertian approximation (thin, solid black curve) and Hilton (1992) empirical fit to photometry of Venus (thin, dashed black curve). The thin, dot-dashed black curve indicates the ratio between Lambertian and Hilton phase functions. Rayleigh-scattered polarization as a function of phase angle (thick, dashed gray curve) and the product of Rayleigh scattering and the Lambertian phase function for spatially unresolved planets (thick, solid gray curve) are shown. The gray arrows indicate that while Rayleigh scattering maximizes the polarization from spatially resolved planets at a $\Theta = 90°$ scattering angle, phase angle effects are expected to drive peak exoplanet polarization toward $\alpha \approx 70°$ for spatially unresolved planets. The product of Rayleigh scattering and the Hilton (1992) phase function (not plotted above for clarity) decreases both peak exoplanet polarization (from 40% to 31%) and phase angle of peak polarization (from 73° to 69°) with respect to the Lambertian phase function.

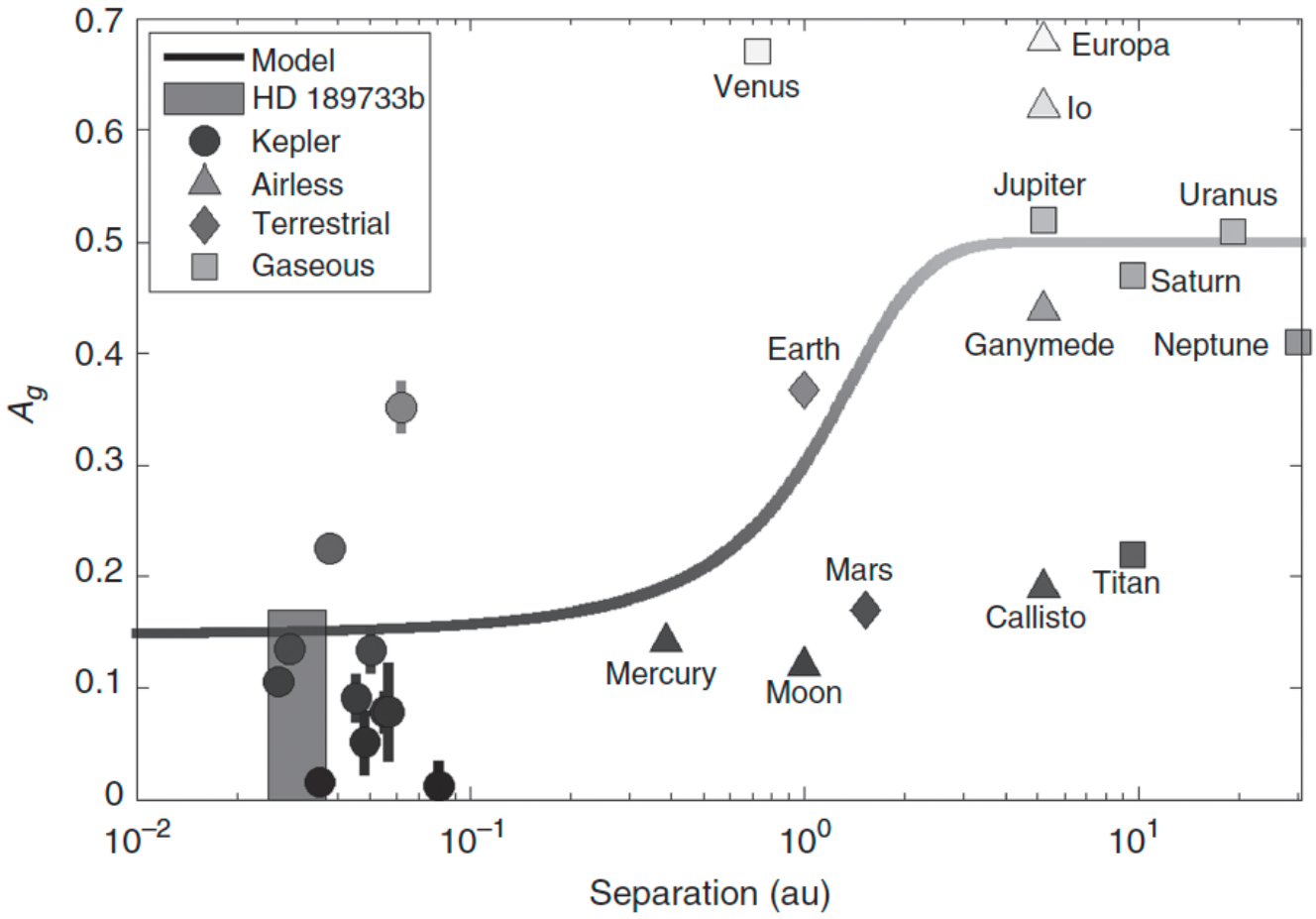

FIGURE 25.5 Theoretical 500 nm geometric albedo, A_g, as a function of star–planet separation (Sudarsky *et al.* 2005). Overplotted are observations of solar system bodies and exoplanets at similar wavelengths. Observations of exoplanets with the Kepler Mission (Heng and Demory 2013) are shown as filled circles, and an upper limit to HD 189733b albedo at ~500 nm (Evans *et al.* 2013) is shown as the filled region in the lower left of the plot (the uncertainty in star–planet separation is greatly magnified for clarity). Evans *et al.* (2013) show that HD 189733b appears to have a detectable albedo at wavelengths shorter than 500 nm.

Signals from rocky exoplanets
Signals from fluid-surface exoplanets

- Moon, Mercury, Mars, and asteroids as proxies for rocky planet polarization
- Negative vs. positive polarization
- Polarization low, challenge for detection
- Spatial variations of polarization across the planetary disk

- Fluid-surface exoplanets give rise to specular reflection
- However, specular reflection carries only a minor amount of radiative energy
- Major challenges for detection

Transit polarimetry

- Polarimetric modulation not only scattering but also due to the transit's effect on stellar polarization
- Stellar limb polarization can reach 12%

$$P(\mu) = P_1\left(\frac{1-\mu^2}{1+k\mu}\right), \quad \mu = \cos\phi,$$

- ϕ angle between surface normal and observer direction
- Transit causes net polarization for the star, even if the star is unpolarized

- The Sun

at 460 nm, $P_1 = 8.7\times10^{-3}$ and $k = 70$

$P_1 = 0.165$ for the Ca I 422.7-nm line

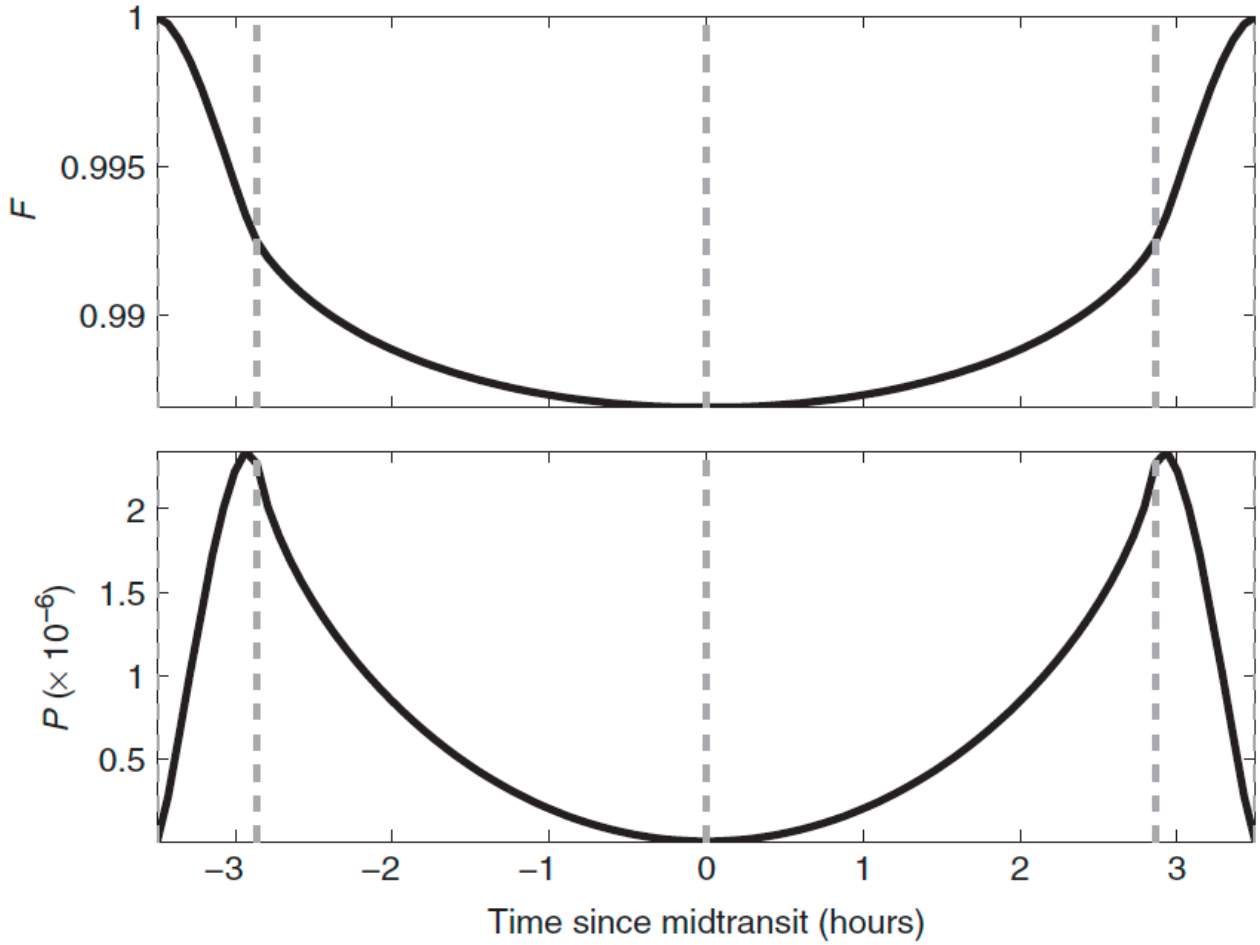

FIGURE 25.6 Modeled 460 nm flux (top) and polarization (bottom) for a 1 R_J planet orbiting a Sun-like star on a circular orbit.

- Limb occultation affects both polarization and polarization position angle for the star
- Scattering plane defined by the radial direction at the limb
- Net polarization parallel
- Polarization position angle parallel to the line joining the centers of the star and planet
- Information about orbital geometry

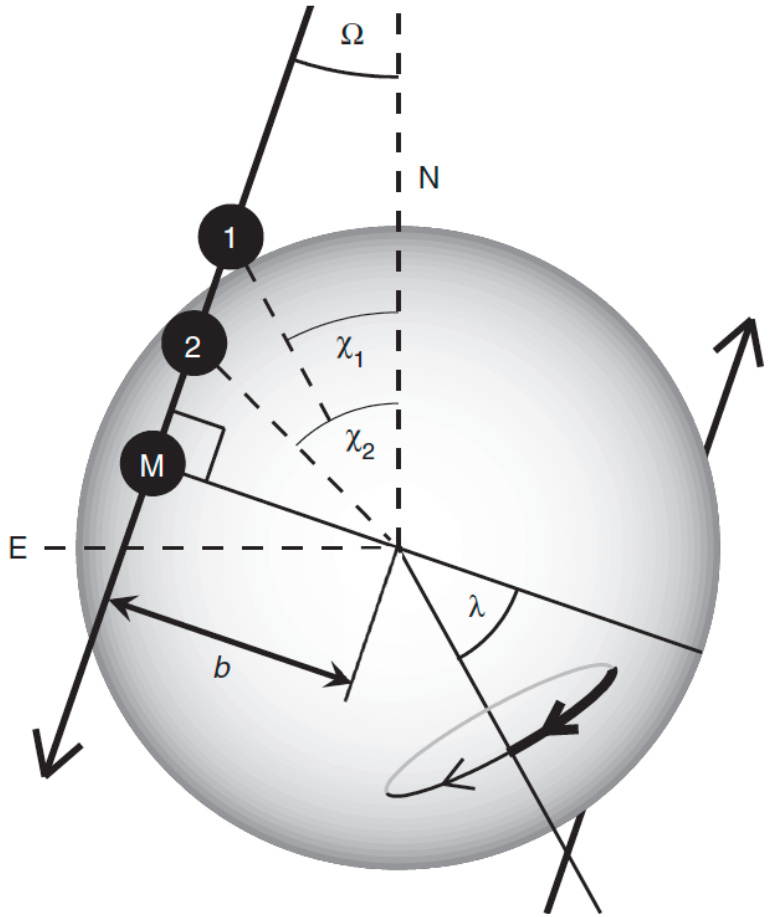

FIGURE 25.7 Geometry of a hypothetical exoplanet transit in polarized light. Exoplanet position on the stellar limb is shown for (1) first contact, (2) second contact, and (M) mid-transit. The position angle of polarization at first and second contacts, χ_1 and χ_2, are shown east of north. The spin–orbit misalignment angle, λ, is shown along with the blue-shifted (thick arrow) and red-shifted (thin arrow) stellar hemispheres. The impact parameter of the transit, b, is also indicated. The planet's orbit is given by black arrows, and the inherent 180° ambiguity in polarization position angle cannot distinguish between transit of the northeast and southwest stellar limbs.

Reproduced from Wiktorowicz and Laughlin (2014) with permission from AAS.

Signals of planetary rings and moons

- Discovery of extrasolar Earth-Moon systems of key importance (role of the Moon as stabilizer)
- Detection of both spatially resolved and unresolved moons possible
- Polarization effects of a spatially unresolved moon not likely to be measurable
- Earth-sized moon orbiting Jupiter-sized exoplanet could allow disk-integrated polarimetric observations with the largest telescopes

The first polarimetric observations of exoplanets

- HD 189733
  - polarized scattered light with DIPol on 0.6-m KVA telescope on la Palma
  - independent confirmation with TurPol at the NOT $\Delta P \approx 10^{-4}$
  - Bounds with Palomar 5-m telescope
  - continued controversy in polarimetric observations vs. other methods
- τ Boötis and 55 Cancri
  - non-detection with WHT
  - upper limit for geometric albedo
  - 3-4 m telescopes not large enough
- υ Andromedae
  - Non-refereed detection with TurPol at the NOT

$$\Delta P = 4 \times 10^{-5}$$

- The role of systematic effects
  - Depending on telescopes, instrument systematics can or cannot be separated from the observed signal

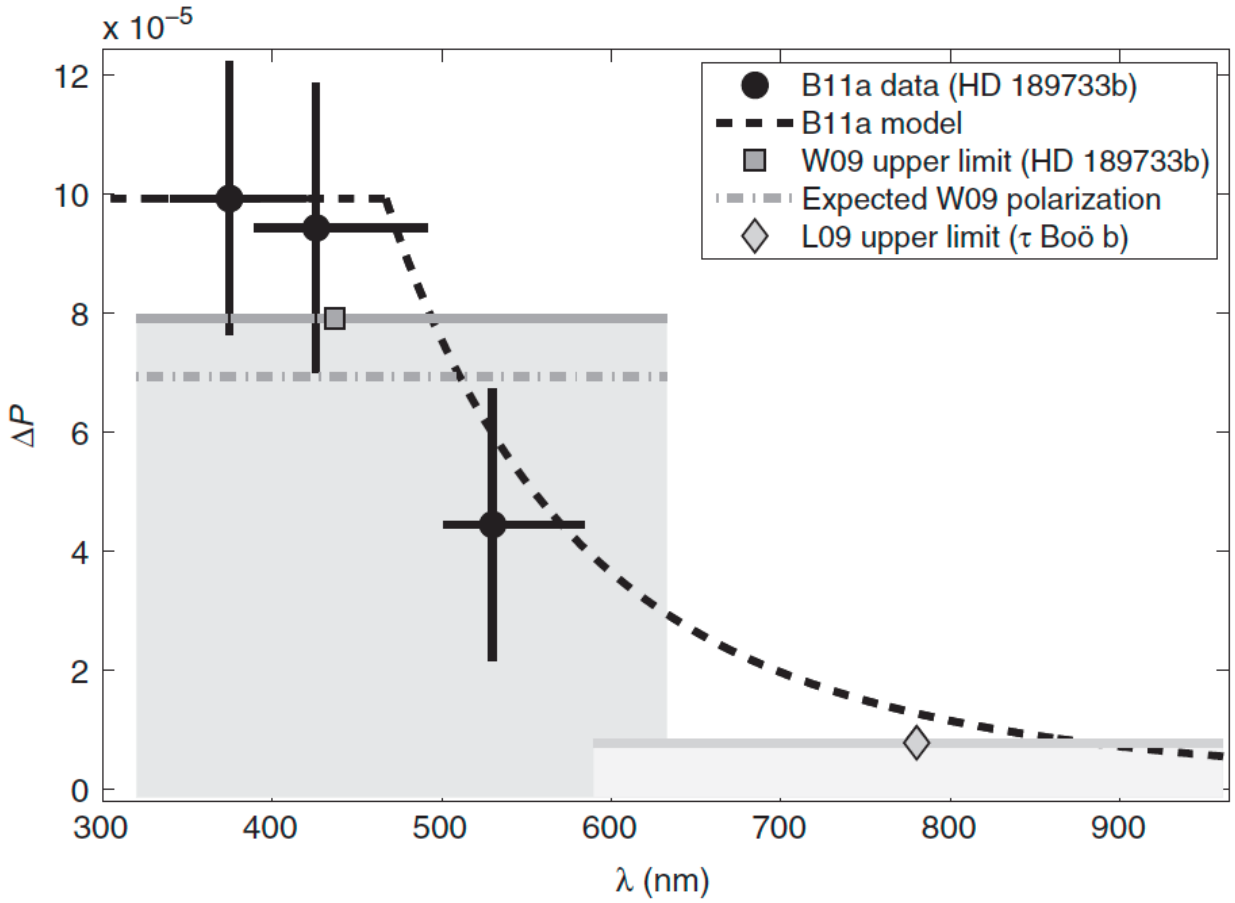

FIGURE 25.8 Comparison of HD 189733b polarization measurements (B11a), a 99% confidence upper limit (W09), and a τ Boö b 99% confidence upper limit (L09).

- Summary of polarimetric detections and bounds

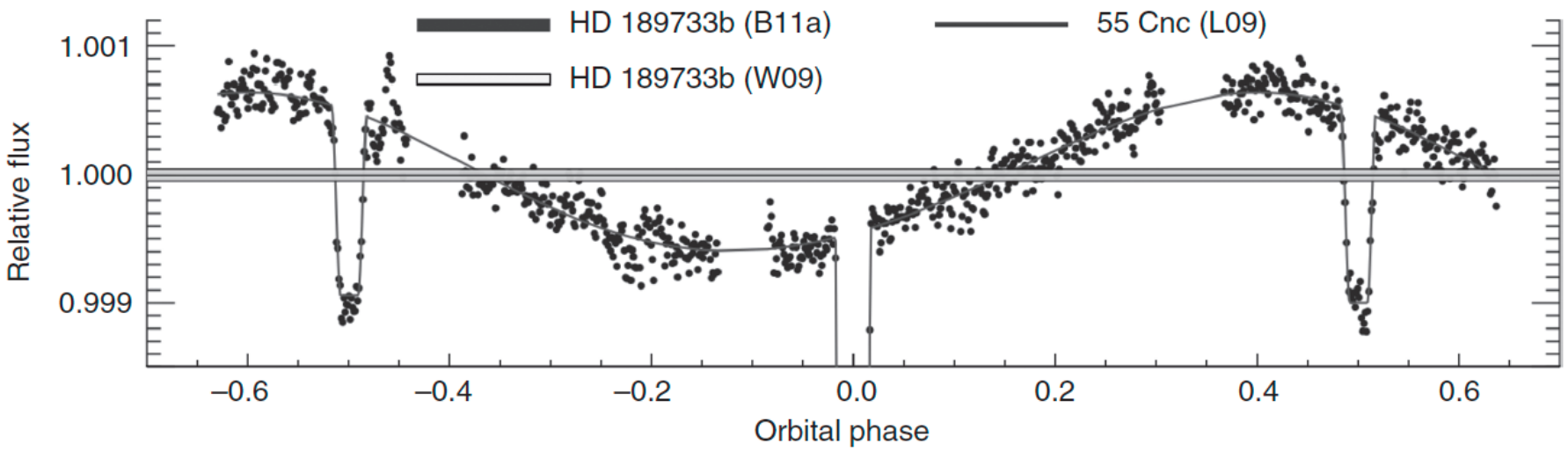

FIGURE 25.9 Comparison of space-based HD 189733b 3.6 μm photometry (K12) with observed B-band polarimetric amplitude (B11a), an upper limit (W09), and the 55 Cnc upper limit (L09) scaled to a 99% confidence interval and in their respective bandpasses (see Fig. 25.8).

Adapted from Knutson *et al.* (2012), Figure 5 with permission © AAS.

- For parts of the orbital phase, polarimetry can be more sensitive than photometry

Polarimetry of Earthshine

- Earthshine on the Moon allows for studies of the Earth as an exoplanet
- Backscattering from the Moon
- Peak polarization at 10%
- Red edge detected, due to rapid brightening of vegetation for wavelengths >700 nm
- Primary challenge is the absence of a full, polarimetric scattering model for the lunar regolith
- Prospects for a remedy on our present course

Conclusions

- Spatially unresolved planets
  - at the edge of detectability
  - systematics to be tackled
- Spatially resolved planets
  - thermal emission observations with Gemini and VLT
- Transiting Exoplanet Survey Satellite (TESS)
  - launch 2018, mission completed in 2020
  - 2100 candidate exoplanets detected
- The future
  - Plato (launch 2026)
  - Thirty Meter Telescope (TMT, first light 2027)
  - European Extremely Large Telescope (E-ELT, first light 2025)